# Spin wave propagation in a uniformly biased curved magnonic waveguide

A. V. Sadovnikov,[1,2,*] C. S. Davies,[3] V. V. Kruglyak,[3] D. V. Romanenko,[1] S. V. Grishin,[1] E. N. Beginin,[1] Y. P. Sharaevskii,[1] and S. A. Nikitov[1,2]

[1]*Laboratory "Metamaterials", Saratov State University, Saratov 410012, Russia*
[2]*Kotel'nikov Institute of Radioengineering and Electronics, Russian Academy of Sciences, Moscow 125009, Russia*
[3]*School of Physics, University of Exeter, Stocker Road, Exeter EX4 4QL, United Kingdom*

Using Brillouin light scattering microscopy and micromagnetic simulations, we study the propagation and transformation of magnetostatic spin waves across uniformly biased curved magnonic waveguides. Our results demonstrate that the spin wave transmission through the bend can be enhanced or weakened by modifying the distribution of the inhomogeneous internal magnetic field spanning the structure. Our results open up the possibility of optimally molding the flow of spin waves across networks of magnonic waveguides, thereby representing a step forward in the design and construction of the more complex magnonic circuitry.

The transmission of optical signals across junctions of planar photonic waveguides and sharp corners can be achieved using turning mirrors [1], photonic crystals [2], and specially designed waveguides featuring either strongly contrasting refractive index [3] or plasmonic properties [4]. This transmission is assisted by the isotropy of the photonic dispersion. Magnetostatic spin waves, in contrast, are inherently anisotropic, possessing dispersion that depends drastically on the relative orientation of the magnetization and wave vector [5]. The anisotropy renders the task of guiding spin waves in conduits of magnetic material (magnonic waveguides) much more complex. Due primarily to the fact that spin waves are free of the Joule heating associated with electronics, they have been suggested to serve as information carriers within beyond-CMOS (complementary metal-oxide semiconductor) computing technologies [6]. So, an entire field of research has emerged devoted to the design and construction of magnonic devices. Minimization of both the spatial footprint of such circuitry and loss associated with the transport of spin waves along waveguides with broken translational symmetry (i.e., at bends) is central to the design of future magnonic computational architectures [7–9].

The foundational concepts of spin wave propagation are fairly well understood [5]. In an in-plane magnetized uniform thin film, the propagating magnetostatic (long-wavelength) spin waves can be classified into two types. If the magnetization is orthogonal to the wave vector, the spin waves have positive dispersion and are referred to as magnetostatic surface spin waves (MSSWs). If the magnetization is parallel to the wave vector, the spin waves have negative dispersion and are typecast as backward-volume magnetostatic spin waves (BVMSWs). In a translationally invariant film, the two dispersions have no overlap. Upon restricting the thin film so as to form a waveguide, the spin waves form laterally confined width modes, having sinusoidal transverse dynamic magnetization with $n$ antinodes. The dispersion branches characterizing the multiple width modes shift in frequency, leading to an overlap of the branches corresponding to the MSSWs and BVMSWs and enabling conversion of the

spin wave type in T junctions of magnonic waveguides [10,11].

Modifications to the shape of a straight magnonic waveguide results in the formation of inhomogeneous distributions of demagnetizing fields, magnetization, and permeability across the structure [12–16]. This broken translational symmetry leads to the scattering and reflection of propagating spin waves, along with the possibility of a width-mode conversion. Generally, an analytical description of spin wave propagation across a curved magnonic waveguide is impossible to formulate unless some strong simplistic approximations are made [17].

Magneto-optical imaging experiments and micromagnetic calculations have been extensively used in recent years to investigate the character of spin wave propagation across magnonic bends featuring different geometries of bending [12,18–22]. This research has been restricted, however, to bends composed of metallic films, such as Permalloy. Insulating magnetic materials, such as yttrium iron garnet (YIG), possess significantly smaller magnetic damping compared to magnetic metals, and it has been recently demonstrated that this small damping persists even when the thickness of YIG is reduced to tens of nanometers [23,24]. This suggests a possibility of using irregular YIG magnonic waveguides within all-magnonic insulator-based technology.

The majority of studies referenced above used a spatially varying bias magnetic field to magnetize the magnonic waveguide. This leaves open a difficult question as to how this mechanism can be effectively downscaled, since stray fields are notoriously difficult to confine on the micrometer and nanometer length scales. Only few studies have considered how spin waves propagate in a waveguide biased by a uniform magnetic field—such a stray field is much easier to practically deliver, upon miniaturization of the waveguide.

Here, we discuss the results of an experimental and numerical investigation into how spin waves propagate across a uniformly biased, geometrically curved magnonic waveguide, composed of YIG. The propagation is studied using a combination of microwave transmission measurements, Brillouin light scattering (BLS) microscopy [25], and micromagnetic simulations [26]. We show that the transmission can be substantially enhanced through the modification of the spatial
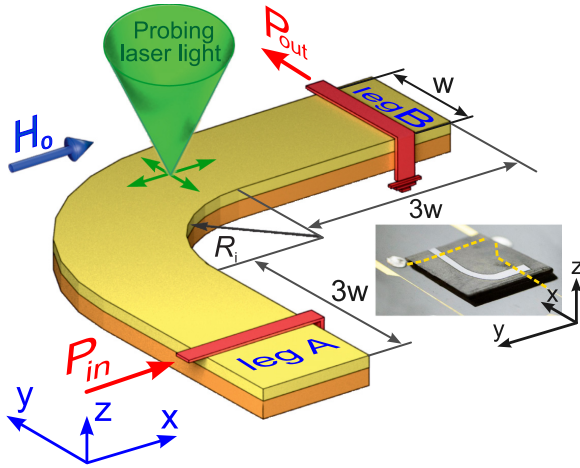
*Corresponding author: SadovnikovAV@gmail.com

FIG. 1. Schematic of the experimental setup used to study the spin wave transmission across the curved waveguide (of thickness 10 $\mu$m). The static magnetic field $H_0 = 1150$ Oe was rotated by $\varphi$ relative to the $x$ axis. Inset: Illustration of the fabricated microstrip transmission line overlaid on the curved YIG waveguide/GGG substrate.

distribution of the internal magnetic field across the waveguide. These results demonstrate that a careful design of magnonic systems can significantly improve the transport of spin waves across magnonic circuitry.

A cartoon of the experimental setup is shown in Fig. 1(a). The YIG structure was fabricated by laser scribing an epitaxially grown 10-$\mu$m-thick film of YIG ($Y_3Fe_5O_{12}$) with a saturation magnetization $M_0 = 139$ G. The curved waveguide had a constant width $w = 470\,\mu$m, an inner radius of curvature $R_i = 2.5w$, and was formed on a substrate of 500-$\mu$m-thick gadolinium gallium garnet ($Gd_3Ga_5O_{12}$, GGG) [27]. Henceforth in this Rapid Communication, we refer to the sections of the YIG waveguide before and after the bend as the "input arm" and "output arm", respectively. Throughout the experiments discussed here, spin waves were excited at the base of the input arm using a microstrip. The input and output microwave transducers, of width $w_{ms} = 30\,\mu$m and length $l_{ms} = 1$ mm, were laid on top of a 250-$\mu$m-thick wafer of polycrystalline corundum (polycor) (upon which the GGG substrate was similarly mounted), as depicted by the dashed line in the inset of Fig. 1. A spatially uniform static magnetic field $H_0 = 1150$ Oe was applied in the plane of the YIG structure, canted at an angle $\varphi$ relative to the $x$ direction.

This system geometry leads to the input transducer exciting MSSWs along the input arm [28,29]. The solid blue curve in Fig. 2(a) shows the transmission response (the absolute value of $S_{21}$) recorded using the vector network analyzer across the output arm with a frequency resolution of 0.02 MHz. Here, it is evident that spin wave width modes are being detected [30,31], whereby the distinct peaks in the measured transmission signal correspond to spin waves boasting a different number of antinodes across their lateral profile. The frequency of the ferromagnetic resonance for the in-plane magnetized stripe [32] can be calculated as $f_0 = \gamma\sqrt{H_i(H_i + 4\pi M_0)} = 5.044$ GHz, where $\gamma/2\pi = 2.8$ MHz/Oe is the electronic gyromagnetic ratio, and $H_i = 1128$ Oe is the internal magnetic field calculated at the center of the input arm from micromagnetic
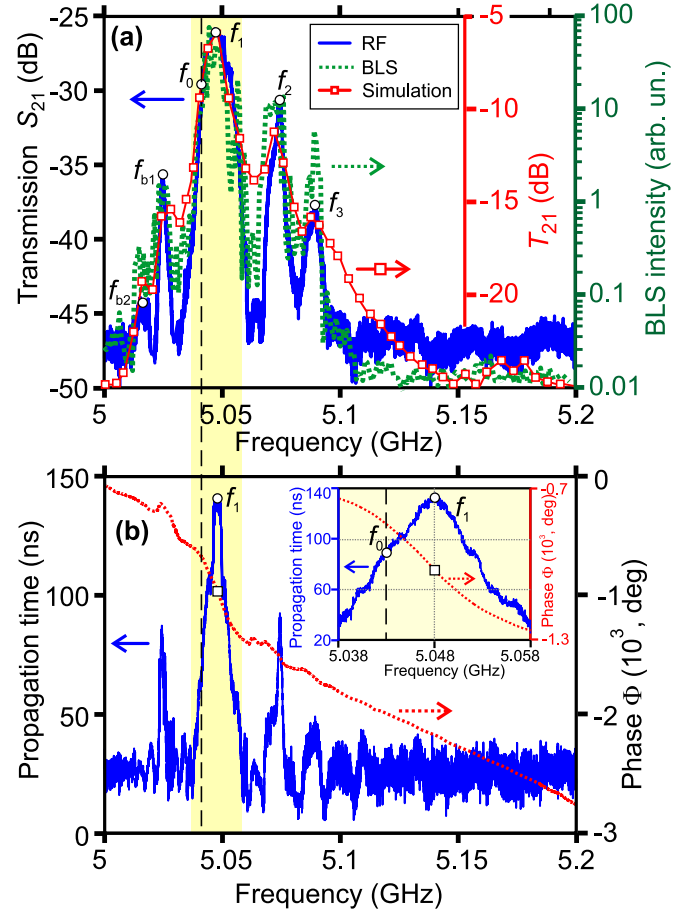


FIG. 2. (a) Transmission characteristics measured at the end of output arm, obtained using a signal network analyzer (solid blue line), BLS microscopy (dashed green line), and micromagnetic simulations (red line with open circles). (b) Frequency dependence of propagation time (blue solid curve) and phase-frequency response (red dotted curve), both measured using a vector network analyzer. The frequency of ferromagnetic resonance $f_0$ is denoted by the vertical dashed line, and all data shown here were obtained with $H_0 = 1150$ Oe applied along the $x$ axis (i.e., $\varphi = 0°$). The shaded yellow area indicates the frequency region which displayed maximum transmission across the bend, and is shown in the inset of (b) with a zoomed frequency scale.

simulations. The two peaks at the frequencies $f_{b1}$ and $f_{b2}$, below $f_0$, originate from the high-order MSSW width modes (modes described laterally in the input arm by $k_x = n\pi/w$) that are excited within the input arm, i.e., the modes with $n = 1$ and $n = 2$ antinodes across their transverse dynamic magnetization profile, respectively [30]. At the frequencies above $f_0$, the $n$th resonant peak in the transmission signal corresponds to the $n$th BVMSW width mode propagating across the output arm (modes described laterally by $k_y = n\pi/w$). The physical interpretation of these data is based on the dispersive conversion of the propagating spin wave. Specifically, the MSSW propagating along the input arm converts to multiple BVMSWs [10], of different orders, propagating along the output arm. This is enabled by the overlap of the surface and volume spin wave bands, originating from the static demagnetization across the input arm [11], the

magnetocrystalline anisotropy of YIG [33], and the lateral confinement of the propagating spin waves.

Microwave measurements also support the argument that MSSWs propagating in the input arm convert to BVMSWs propagating in the output arm. The frequency dependence of the propagation time $\tau(f)$ and the phase-frequency response $\Phi(f)$ of the microstrip line with the curved magnonic waveguide are indicated by the blue-solid and red-dashed lines in Fig. 2(b), respectively. It is well known that the propagation time (inversely proportional to the group velocity) for MSSWs and BVMSWs increases and decreases, respectively, upon increasing the excitation frequency [33,34]. Across the curved magnonic waveguide, both MSSWs and BVMSWs are propagating. This leads to the formation of the peak at the frequency $f_1$ [Fig. 2(b)], which also corresponds to the maximum of the transmission [Fig. 2(a)]. At the frequencies

lower than $f_1$, the time-delay dependence corresponds to the MSSW, i.e., $\tau$ is increased with the frequency increase. The value of $\tau$ is almost constant in the vicinity of $f_1$, and is reduced at the frequencies higher than $f_1$. The latter behavior is typical for BVMSWs [33]. To verify the frequency dependence of propagation time for MSSW and BVMSV we performed a separate measurement of the spin wave propagation time in the input and output arms (see Supplemental Material [35]).

The fact of the propagation of both types of the spin waves was also confirmed by the measurement of the phase-frequency response $\Phi(f)$ [since $\tau = d\Phi(f)/df$]. The inset of Fig. 2(b) shows, with higher resolution, the dependencies of $\tau(f)$ and $\Phi(f)$ in the vicinity of $f_1$. From these data one can conclude that the observed resonant peak corresponds to the nondispersive spin wave propagation in the curved magnonic waveguide [36,37]. These findings are important
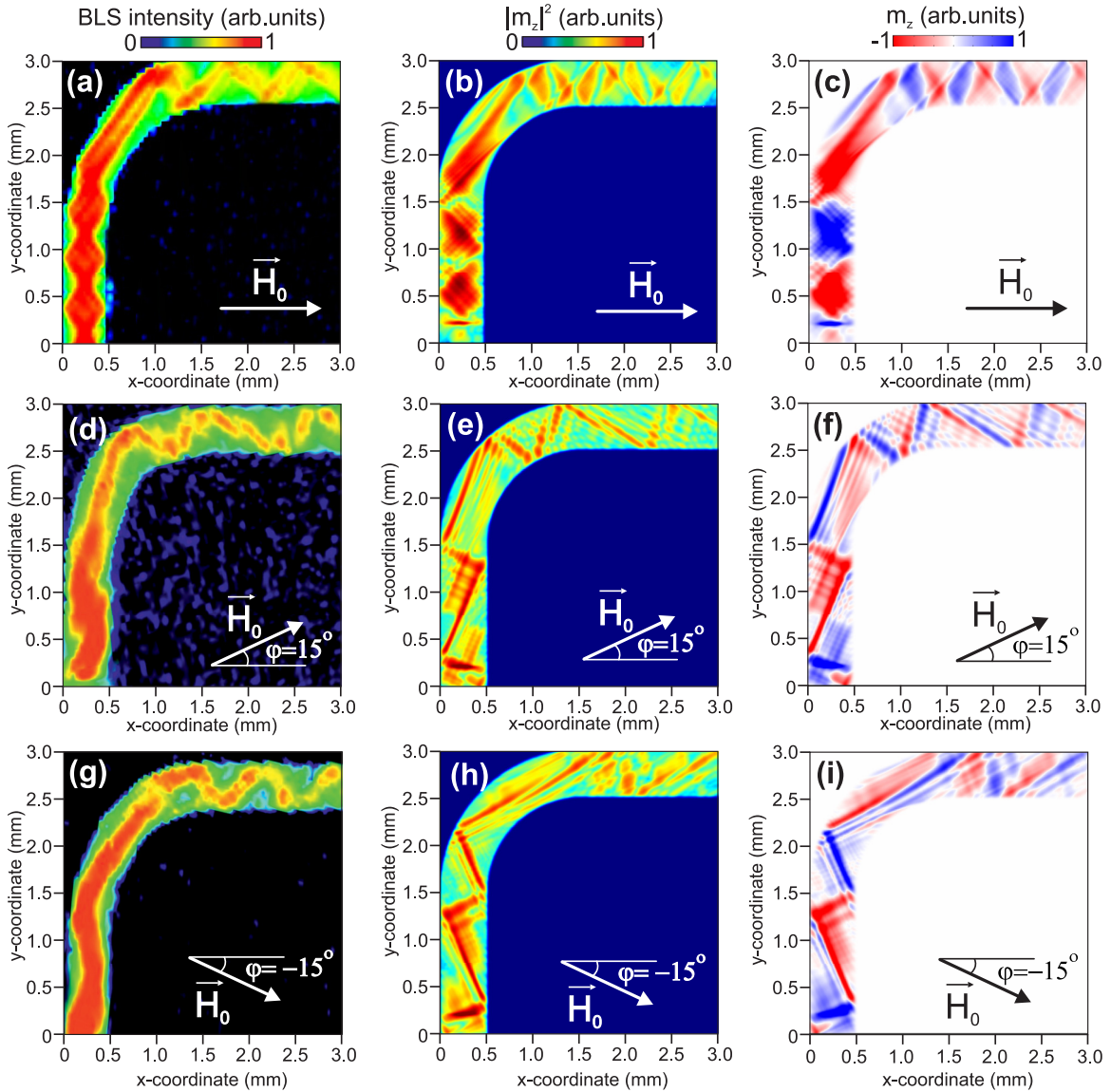


FIG. 3. Amplitude-resolved BLS maps [left column, (a), (d), and (g)], simulated BLS-like maps [middle column, (b), (e), and (h)], and simulated snapshots of the dynamic out-of-plane component of magnetization [right column, (c), (f), and (i)]. The spin wave propagation is mapped in all panels with the frequency $f_1 = 5.05\,\text{GHz}$ and bias magnetic field strength $H_0 = 1150\,\text{Oe}$, and with the bias magnetic field orientation as indicated.

to the possible formation of bright and dark temporal solitons [38,39] in the proposed structure.

The propagation path of spin waves across the curved waveguide was imaged using BLS microscopy. The BLS intensity signal is proportional to the square of the amplitude of the magnetization oscillations. The panels in the left column of Fig. 3 show the normalized spatial maps of the BLS intensity that were recorded for different orientations of the static magnetic field, as indicated. Throughout, the probing laser spot was scanned across an area of $(3.0 \times 3.0)$ mm$^2$, with a step size of $25\ \mu$m. The input transmission line carried 100-ns-long bursts of microwave at frequency $f_1 = 5.05$ GHz, with the burst repetition period set to $2\ \mu$s in order to avoid overheating of the YIG sample. Clearly, the highest peak of transmission at $\varphi = 0°$ in the vicinity of frequency $f_1$ corresponds to the simultaneous excitation of both the first and third width modes within the input arm [evidenced by the spatial beating observed in Fig. 3(a)] and transformation of said modes to (predominantly) the first and second width modes in the output arm. To complement and further understand the experimental results, micromagnetic simulations were performed using the Object-Oriented Micro-Magnetic Framework (OOMMF) [26]. These calculations yield both the intensity [Fig. 3(b)] and phase [Fig. 3(c)] of the propagating spin wave. The calculated spin wave intensity maps [Fig. 3(b)] agree qualitatively with the BLS data [Fig. 3(a)]. We emphasize that the spatial distribution of spin wave intensity does not significantly change over the frequency range of the first sideband in the vicinity of $f_1$. The frequency dependence of the spin wave transmission coefficient $T_{21}(f)$ calculated from the micromagnetic simulations shows a good agreement with that obtained by integrating the BLS intensity over the transverse section at the position (2.5 mm $< y <$ 3.0 mm at $x = 3.0$ mm) of the output microstrip antenna [Fig. 2(a)]. The frequency resolution in the BLS microscopy measurements, defined by the microwave generator, was 2 MHz.

To investigate how the spin wave transmission was affected by the orientation of $H_0$, further experiments and micromagnetic simulations were performed for various in-plane field angles $\varphi$. The results obtained for $\varphi = 15°$ and $-15°$ are shown in the middle and lower rows of Fig. 3, respectively. We first note that the experimental and numerical results show that the deviation of the bias magnetic field away from the $x$ axis leads to the excitation of both the first and second MSSW modes in the input arm. This is anticipated due to the breaking of the symmetry of the magnetization across the width of the input arm, with respect to the edges of the waveguide [12]. To study more quantitatively the transmission of the spin wave with the variation of angle $\varphi$, we plot the maximum of the transmission coefficient as a function of $\varphi$ [Fig. 4(a)]. All spectra in Fig. 4(a) were obtained through integrating the BLS signal (acquired at the frequency $f_1 = 5.05$ GHz) over the region 2.5 mm $< y <$ 3.0 mm at $x = 3.0$ mm.

Intuitively, one may expect that the transmission coefficient reaches its maximum value when $\varphi = 0°$. However, we repeatedly observed that the strongest spin wave transmission across the magnonic bend was achieved when $\varphi = -15°$, with the enhancement (relative to the transmission obtained when $\varphi = 0°$) reaching a factor of 2 (i.e., a logarithmic difference of 3 dB).

To explain the observed nontrivial angular dependence of the transmission, one might invoke two effects. The first
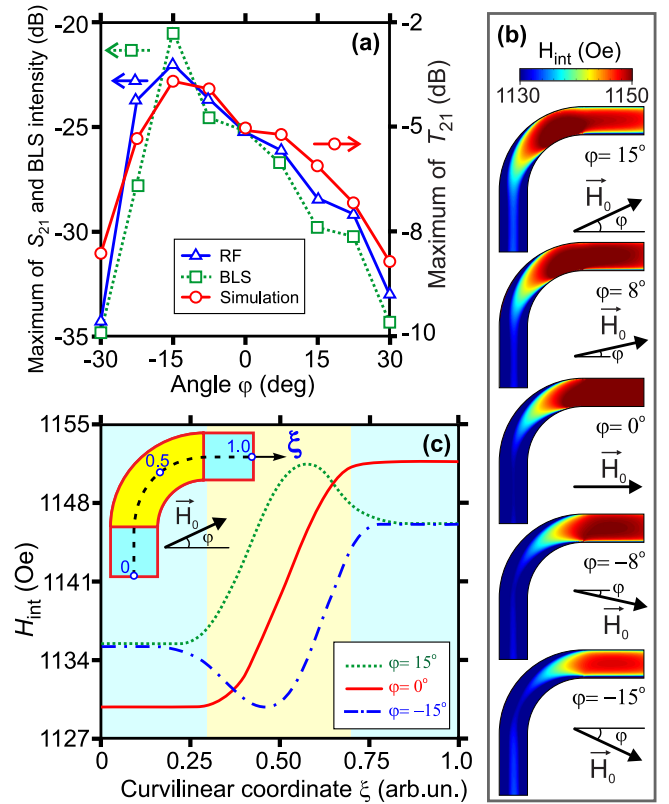


FIG. 4. (a) The efficiency of spin wave transmission across the curved bend as a function of the bias orientation, as measured using a signal network analyzer (blue triangles), BLS microscopy (green squares), and micromagnetic calculations (red circles). (b) Top to bottom: The spatial distribution of the internal field across the curved bend, for varying angles of $H_0$. (c) The amplitude of the internal magnetic field as a function of the curvilinear coordinate $\xi$ (the definition of which is shown in the inset) at varying angles of bias, as indicated.

concerns the interpretation of the observed spin wave propagation. Usually (and so far in this Rapid Communication), the spin waves propagating across the waveguides have been exclusively considered as laterally confined modes. However, it is equally valid to consider this as a spin wave beam that undergoes multiple reflections from the geometrical edges of the waveguide, according to the (generally anisotropic) laws of spin wave optics [40–42]. With this interpretation in mind, a comparison of the middle and lower panels of Fig. 3(a) shows that the spin wave beam undergoes fewer reflections from the waveguide's edges when $\varphi = -15°$, compared to when $\varphi = +15°$. Thus, the transmission is enhanced when $\varphi = -15°$, compared to when $\varphi = +15°$. However, this interpretation does not appear to explain the improved transmission at $\varphi = -15°$ in comparison to the case of $\varphi = 0°$.

The second effect that we consider involves the spatial variation of the static internal field across the curved bend. To study this, we performed micromagnetic simulations in order to quantitatively evaluate this variation, and the results are shown in Fig. 4(b). The internal field is plotted for the center of the waveguide [as defined in the inset of Fig. 4(b)] as a function of the length coordinate along the

middle of the waveguide. We can see that, when $\varphi = 0°$, the internal field increases monotonically and smoothly from $H_{int1} = 1128$ Oe to $H_{int2} = 1150$ Oe across the curved bend. This provides the possibility for spin waves to efficiently convert from MSSW into BVMSW in the frequency range between $f_{start} = \gamma \sqrt{H_{int1}(H_{int1} + 4\pi M_0)} = 5.044$ GHz and $f_{end} = \gamma \sqrt{H_{int2}(H_{int2} + 4\pi M_0)} = 5.113$ GHz. The values of $f_{start}$ and $f_{end}$ confine the distinguishable frequency region of the spin wave transmission response [apparent in Fig. 2(a)].

Figure 4(b) summarizes the results of the internal field calculation, showing how the inhomogeneous distribution of the static internal magnetic field in the curved area depends on the orientation of the bias magnetic field. In particular, we observe that, by rotating the bias magnetic field away from $\varphi = 0°$, we can induce either a local enhancement ($\varphi = 15°$) or reduction ($\varphi = -15°$) in the static internal field distribution in the curved region [Fig. 4(c)]. We can therefore use the interpretation from Ref. [43] to understand the transmission enhancement at $\varphi = -15°$ observed here. In Ref. [43], Demokritov *et al.* considered the propagation of BVMSWs across a similar local field inhomogeneity and observed that the BVMSW was transmitted (reflected) when propagating across a local enhancement (reduction) in the internal field. Instead, we find that the opposite is true for propagating MSSWs, whereby the MSSW is transmitted (reflected) by a local reduction (enhancement) in the internal field. From a consideration of the dispersion characterizing MSSWs, it is evident that a region with a slightly enhanced local internal field decreases the wave number of the MSSW, and can indeed contain a turning point for a MSSW [44–47], whereas

the local minor decrease of $H_{int}(\varphi)$ leads to the increase of the MSSW's wave number. The latter is better supported by the magnonic waveguide, hence explaining the improved transmission.

In conclusion, we have shown that the propagation of spin waves across a curved magnonic waveguide is strongly correlated with the profile of the internal field. In particular, the measurements and their analysis presented in this Rapid Communication demonstrate that the spin wave transmission through a magnonic waveguide bend can be either enhanced or reduced by tuning the orientation of the magnetization. We speculate that the reverse mechanism could also be true: If the input arm supports BVMSWs (such that $\varphi = 90°$), a similar enhancement or reduction of the spin wave transmission could be achieved through a modest rotation of the bias magnetic field. Furthermore, we believe that our findings can be applied in the future design of nanoscale magnonic devices to be fabricated from ultrathin YIG films, where the propagating spin waves will still retain some dispersive anisotropy from the dipolar interaction.

[1] Y. Chung and N. Dagli, Experimental and theoretical study of turning mirrors and beam splitters with optimized waveguide structures, Opt. Quantum Electron. **27**, 395 (1995).

[2] S. Y. Lin, E. Chow, V. V. Hietala, P. R. Villeneuve, and J. D. Joannopoulos, Experimental demonstration of guiding and bending of electromagnetic waves in a photonic crystal, Science **282**, 274 (1998).

[3] M. Cherchi, S. Ylinen, M. Harjanne, M. Kapulainen, and T. Aalto, Dramatic size reduction of waveguide bends on a micron-scale silicon photonic platform, Opt. Express **21**, 17814 (2013).

[4] W. Wang, Q. Yang, F. Fan, H. Xu, and Z. L. Wang, Light propagation in curved silver nanowire plasmonic waveguides, Nano Lett. **11**, 1603 (2011).

[5] A. G. Gurevich and G. A. Melkov, *Magnetization Oscillations and Waves* (CRC Press, New York, 1996).

[6] http://www.itrs2.net, accessed 31/05/2016.

[7] V. V. Kruglyak, S. O. Demokritov, and D. Grundler, Magnonics, J. Phys. D: Appl. Phys. **43**, 264001 (2010).

[8] A. A. Serga, A. V. Chumak, and B. Hillebrands, YIG magnonics, J. Phys. D: Appl. Phys. **43**, 264002 (2010).

[9] S. A. Nikitov, D. V. Kalyabin, I. V. Lisenkov, A. N. Slavin, Yu. N. Barabanenkov, S. A. Osokin, A. V. Sadovnikov, E. N. Beginin, M. A. Morozova, Yu. P. Sharaevsky, Yu. A. Filimonov, Yu. V. Khivintsev, S. L. Vysotsky, V. K. Sakharov, and E. S. Pavlov, Magnonics: A new research area in spintronics and spin wave electronics, Phys.-Usp. **58**, 1002 (2015).

[10] T. Brächer, P. Pirro, J. Westermann, T. Sebastian, B. Lägel, B. Van de Wiele, A. Vansteenkiste, and B. Hillebrands, Generation

of propagating backward volume spin waves by phase-sensitive mode conversion in two-dimensional microstructures, Appl. Phys. Lett. **102**, 132411 (2013).

[11] A. V. Sadovnikov, C. S. Davies, S. V. Grishin, V. V. Kruglyak, D. V. Romanenko, Yu. P. Sharaevskii, and S. A. Nikitov, Magnonic beam splitter: The building block of parallel magnonic circuitry, Appl. Phys. Lett. **106**, 192406 (2015).

[12] P. Clausen, K. Vogt, H. Schultheiss, S. Schäfer, B. Obry *et al.*, Mode conversion by symmetry breaking of propagating spin waves, Appl. Phys. Lett. **99**, 162505 (2011).

[13] R. Gieniusz, H. Ulrichs, V. D. Bessonov, U. Guzowska, A. I. Stognii, and A. Maziewski, Single antidot as a passive way to create caustic spin-wave beams in yttrium iron garnet films, Appl. Phys. Lett. **102**, 102409 (2013).

[14] E. N. Beginin, A. V. Sadovnikov, Y. P. Sharaevsky, and S. A. Nikitov, Multimode surface magnetostatic wave propagation in irregular planar YIG waveguide, Solid State Phenom. **215**, 389 (2014).

[15] C. S. Davies, A. Francis, A. V. Sadovnikov, S. V. Chertopalov, M. T. Bryan, S. V. Grishin, D. A. Allwood, Y. P. Sharaevskii, S. A. Nikitov, and V. V. Kruglyak, Towards graded-index magnonics: Steering spin waves in magnonic networks, Phys. Rev. B **92**, 020408 (2015).

[16] C. S. Davies, A. V. Sadovnikov, S. V. Grishin, Y. P. Sharaevsky, S. A. Nikitov, and V. V. Kruglyak, Field-controlled phase-rectified magnonic multiplexer, IEEE Trans. Magn. **51**, 3401904 (2015).

[17] V. S. Tkachenko, A. N. Kuchko, and V. V. Kruglyak, An effect of the curvature induced anisotropy on the spectrum of spin waves in a curved magnetic nanowire, Low Temp. Phys. **39**, 163 (2013).

[18] S. Bance, T. Schrefl, G. Hrkac, A. Goncharov, D. A. Allwood, and J. Dean, Micromagnetic calculation of spin wave propagation for magnetologic devices, J. Appl. Phys. **103**, 07E735 (2008).

[19] M. Dvornik, Y. Au, and V. V. Kruglyak, *Micromagnetic Simulations in Magnonics*, Magnonics: From Fundamentals to Applications (Springer Science & Business Media, 2013), Vol. 125, pp. 101–115.

[20] X. Xing, Y. Yu, S. Li, and X. Huang, How do spin waves pass through a bend? Sci. Rep. **3**, 2958 (2013).

[21] X. Xing, W. Yin, and Z. Wang, Excitation of antisymmetric modes and modulated propagation of spin waves in bent magnonic waveguides, J. Phys. D: Appl. Phys. **48**, 215004 (2015).

[22] K. Vogt, H. Schultheiss, S. Jain, J. E. Pearson, A. Hoffmann, S. D. Bader, and B. Hillebrands, Spin waves turning a corner, Appl. Phys. Lett. **101**, 042410 (2012).

[23] M. Evelt, V. E. Demidov, V. Bessonov, S. O. Demokritov, J. L. Prieto, M. Muñoz, J. Ben Youssef, V. V. Naletov, G. de Loubens, O. Klein, M. Collet, K. Garcia-Hernandez, P. Bortolotti, V. Cros, and A. Anane, High-efficiency control of spin-wave propagation in ultra-thin yttrium iron garnet by the spin-orbit torque, Appl. Phys. Lett. **108**, 172406 (2016).

[24] L. V. Lutsev, A. M. Korovin, V. E. Bursian, S. V. Gastev, V. V. Fedorov, S. M. Suturin, and N. S. Sokolov, Low-relaxation spin waves in laser-molecular-beam epitaxy grown nanosized yttrium iron garnet films, Appl. Phys. Lett. **108**, 182402 (2016).

[25] S. O. Demokritov and V. E. Demidov, Micro-Brillouin light scattering spectroscopy of magnetic nanostructures, IEEE Trans. Magn. **44**, 6 (2008).

[26] M. J. Donahue and D. G. Porter, National Institute of Standards and Technology Interagency Report No. NISITR 6376, 1999 (unpublished).

[27] S. Sheshukova, E. Beginin, A. V. Sadovnikov, Y. Sharaevsky, and S. A. Nikitov, Multimode propagation of magnetostatic waves in a width-modulated yttrium-iron-garnet waveguide, IEEE Magn. Lett. **5**, 3700204 (2014).

[28] S. N. Bajpai, Excitation of magnetostatic surface waves: Effect of finite sample width, J. Appl. Phys. **58**, 910 (1985).

[29] R. W. Damon and J. Eschbach, Magnetostatic modes of a ferromagnet slab, J. Phys. Chem. Solids **19**, 308 (1961).

[30] T. W. O'Keefe and R. W. Patterson, Magnetostatic surface-wave propagation in finite samples, J. Appl. Phys. **49**, 4886 (1978).

[31] J. Jorzick, S. O. Demokritov, C. Mathieu, B. Hillebrands, B. Bartenlian, C. Chappert, F. Rousseaux, and A. N. Slavin, Brillouin light scattering from quantized spin waves in micron-size magnetic wires, Phys. Rev. B **60**, 15194 (1999).

[32] C. Kittel, Ferromagnetic resonance, J. Phys. Rad. **12**, 291 (1951).

[33] I. V. Zavislyak, V. M. Talaevskii, and L. V. Chevnyk, Anisotropy-induced features in magnetostatic wave spectra, Fiz. Tverd. Tela **31**, 319 (1989).

[34] S. D. Adam and M. R. Daniel, The status of magnetostatic devices, IEEE Trans. Magn. **17**, 6 (1981).

[35] See Supplemental Material at http://link.aps.org/supplemental/10.1103/PhysRevB.96.060401 for additional details about the propagation time of the spin waves navigating the magnonic bend, and also a description of the micromagnetic methodology.

[36] Here, the phrase "nondispersive spin wave propagation" refers to the fact that the overall phase shift of the spin wave, at the end of the output arm, is constant. This has arisen because the spin waves propagating in the input and output arm have a phase shift that increases and decreases, respectively. Thus, the overall phase shift can compensate each other, and so one would observe a spin wave pulse that conserves its form after navigating the curved waveguide (if damping is neglected).

[37] F. R. Morgenthaler, Nondispersive magnetostatic forward volume waves under field gradient control, J. Appl. Phys. **53**, 2652 (1982).

[38] A. A. Serga, A. Andre, S. O. Demokritov, B. Hillebrands, and A. N. Slavin, Black soliton formation from phase-adjusted spin wave packets, J. Appl. Phys. **95**, 6607 (2004).

[39] A. B. Ustinov, B. A. Kalinikos, V. E. Demidov, and S. O. Demokritov, Formation of gap solitons in ferromagnetic films with a periodic metal grating, Phys. Rev. B **81**, 180406 (2010).

[40] A. V. Vashkovsky and E. H. Lock, Properties of backward electromagnetic waves and negative reflection in ferrite films, Phys.-Usp. **49**, 389 (2006).

[41] V. Veerakumar and R. E. Camley, Magnon focusing in thin ferromagnetic films. Phys. Rev. B **74**, 214401 (2006).

[42] T. Schneider, A. A. Serga, A. V. Chumak, C. W. Sandweg, S. Trudel, S. Wolff, M. P. Kostylev, V. S. Tiberkevich, A. N. Slavin, and B. Hillebrands, Nondiffractive Subwavelength Wave Beams in a Medium with Externally Controlled Anisotropy. Phys. Rev. Lett. **104**, 197203 (2010).

[43] S. O. Demokritov, A. A. Serga, A. Andre, V. E. Demidov, M. P. Kostylev, B. Hillebrands, and A. N. Slavin, Tunneling of Dipolar Spin Waves through a Region of Inhomogeneous Magnetic Field, Phys. Rev. Lett. **93**, 047201 (2004).

[44] J. R. Eshbach, Spin-Wave Propagation and the Magnetoelastic Interaction in Yttrium Iron Garnet, Phys. Rev. Lett. **8**, 357 (1962); J. Appl. Phys. **34**, 1298 (1963).

[45] R. W. Damon and H. van de Vaart, Propagation of magnetostatic spin waves at microwave frequencies in a normally-magnetized disk, J. Appl. Phys. **36**, 3453 (1965).

[46] R. W. Damon and H. van de Vaart, Propagation of magnetostatic spin waves at microwave frequencies. II. Rods, J. Appl. Phys. **37**, 2445 (1966).

[47] E. Schlömann and R. I. Joseph, Generation of spin waves in nonuniform dc magnetic fields. II. Calculation of the coupling length, J. Appl. Phys. **35**, 167 (1964).